J|A|C|S ARTICLES

Published on Web 05/21/2009

Location of Inhibitors Bound to Group IVA Phospholipase A_2 Determined by Molecular Dynamics and Deuterium Exchange Mass Spectrometry

John E. Burke,[†] Arneh Babakhani,[†] Alemayehu A. Gorfe,[†] George Kokotos,[⊥] Sheng Li,[‡] Virgil L. Woods, Jr.,[‡] J. Andrew McCammon,[†,§,||] and Edward A. Dennis*[,†,§]

Department of Chemistry and Biochemistry, Department of Medicine and Biomedical Sciences Graduate Program, Department of Pharmacology, and Howard Hughes Medical Institute, University of California, San Diego, 9500 Gilman Drive MC 0601, La Jolla, California 92093-0601, and Department of Chemistry, University of Athens, Panepistimiopolis, Athens 15771, Greece

Received January 8, 2009; E-mail: edennis@ucsd.edu

Abstract: An analysis of group IVA (GIVA) phospholipase A_2 (PLA_2) inhibitor binding was conducted using a combination of deuterium exchange mass spectrometry (DXMS) and molecular dynamics (MD). Models of the GIVA PLA_2 inhibitors pyrrophenone and the 2-oxoamide AX007 docked into the protein were designed on the basis of deuterium exchange results, and extensive molecular dynamics simulations were run to determine protein−inhibitor contacts. The models show that both inhibitors interact with key residues that also exhibit changes in deuterium exchange upon inhibitor binding. Pyrrophenone is bound to the protein through numerous hydrophobic residues located distal from the active site, while the oxoamide is bound mainly through contacts near the active site. We also show differences in protein dynamics around the active site between the two inhibitor-bound complexes. This combination of computational and experimental methods is useful in defining more accurate inhibitor binding sites and can be used in the generation of better inhibitors against GIVA PLA_2.

Introduction

The group IVA phospholipase A_2 (GIVA PLA_2), also known as $cPLA_2$ for cytosolic PLA_2, is a member of the superfamily of phospholipase A_2 enzymes that cleave a fatty acid from the sn-2 position of phospholipids.[1,2] The products of this reaction, a free fatty acid and a lysophospholipid, play important roles as lipid second messengers. GIVA PLA_2 was isolated in 1990 from U937 cells[3] and was discovered to be composed of a C2 domain, and an α/β hydrolase domain containing the active site.[4] The GIVA PLA_2 is specific for phospholipids with arachidonic acid in the sn-2 position, and the release of arachidonic acid is the first step in the production of eicosanoids and leukotrienes, which play important roles in many inflammatory diseases.[5] Experiments performed using mice deficient in the GIVA PLA_2 enzyme have proven that GIVA PLA_2 is the critical PLA_2 enzyme for eicosanoid generation in many inflammatory disease models.[6−8]

The enzyme was shown through site-directed mutagenesis to contain an active site dyad composed of Ser-228 and Asp-549,[9] and this was later confirmed through X-ray crystallography of the enzyme.[10] The enzyme contains an amphipathic lid region from 415−432 that prevents accession of phospholipid into the active site.[10] The lid region has two disordered regions from 408−412 and 433−457 that may act as hinges that allow the lid region to open. It has been shown that this lid is in the open conformation when the enzyme is in the presence of lipid vesicles (its natural substrate) or when inhibitor is bound in the active site.[11]

The knowledge that GIVA PLA_2 plays an important functional role in many inflammatory diseases has sparked an interest

[†] Department of Chemistry and Biochemistry, University of California, San Diego.
[‡] Department of Medicine and Biomedical Sciences Graduate Program, University of California, San Diego.
[§] Department of Pharmacology, University of California, San Diego.
[||] Howard Hughes Medical Institute, University of California, San Diego.
[⊥] University of Athens.

(1) Schaloske, R. H.; Dennis, E. A. *Biochim. Biophys. Acta* **2006**, *1761*, 1246–59.
(2) Six, D. A.; Dennis, E. A. *Biochim. Biophys. Acta* **2000**, *1488*, 1–19.
(3) Clark, J. D.; Milona, N.; Knopf, J. L. *Proc. Natl. Acad. Sci. U.S.A.* **1990**, *87*, 7708–12.
(4) Clark, J. D.; Lin, L. L.; Kriz, R. W.; Ramesha, C. S.; Sultzman, L. A.; Lin, A. Y.; Milona, N.; Knopf, J. L. *Cell* **1991**, *65*, 1043–51.
(5) Funk, C. D. *Science* **2001**, *294*, 1871–1875.
(6) Bonventre, J. V.; Huang, Z.; Taheri, M. R.; O'Leary, E.; Li, E.; Moskowitz, M. A.; Sapirstein, A. *Nature* **1997**, *390*, 622–625.
(7) Nagase, T.; Uozumi, N.; Ishii, S.; Kume, K.; Izumi, T.; Ouchi, Y.; Shimizu, T. *Nat. Immunol.* **2000**, *1*, 42–46.
(8) Uozumi, N.; Kume, K.; Nagase, T.; Nakatani, N.; Ishii, S.; Tashiro, F.; Komagata, Y.; Maki, K.; Ikuta, K.; Ouchi, Y.; Miyazaki, J.; Shimizu, T. *Nature* **1997**, *390*, 618–622.
(9) Pickard, R. T.; Chiou, X. G.; Strifler, B. A.; DeFelippis, M. R.; Hyslop, P. A.; Tebbe, A. L.; Yee, Y. K.; Reynolds, L. J.; Dennis, E. A.; Kramer, R. M.; Sharp, J. D. *J. Biol. Chem.* **1996**, *271*, 19225–19231.
(10) Dessen, A.; Tang, J.; Schmidt, H.; Stahl, M.; Clark, J. D.; Seehra, J.; Somers, W. S. *Cell* **1999**, *97*, 349–60.
(11) Burke, J. E.; Hsu, Y. H.; Deems, R. A.; Li, S.; Woods, V. L., Jr.; Dennis, E. A. *J. Biol. Chem.* **2008**, *283*, 31227–36.

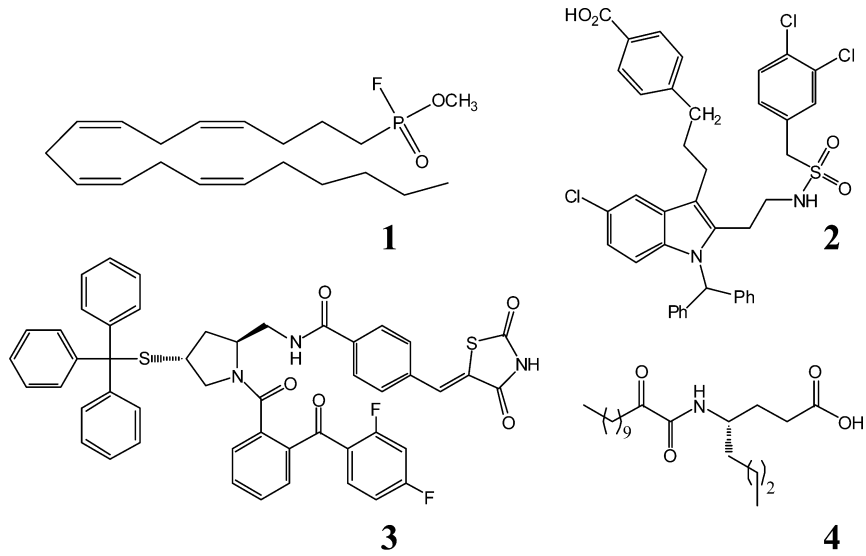

Figure 1. Inhibitors of GIVA PLA_2. (1) MAFP. (2) Efipladib. (3) Pyrrophenone. (4) AX007.

in the production of specific inhibitors against this enzyme. The first inhibitors of this enzyme were based around the specificity of the enzyme for phospholipids with arachidonic acid in the sn-2 position, and as such arachidonyl trifluoromethyl ketones (ATK) and methyl arachidonyl fluorophosphonate (MAFP) (**1**) were synthesized and found to inhibit the enzyme in platelet models of eicosanoid generation.[12−14] In recent years, many different strategies have been pursued to create effective and specific GIVA PLA_2 inhibitors. These have included indole derivatives developed by Wyeth Pharmaceuticals (**2**),[15−18] pyrrolidine-based inhibitors by Shionogi Pharmaceuticals (**3**),[19−22] substituted propan-2-ones by Astra Zeneca and the Lehr group,[23−26] as well as 2-oxoamide compounds by the Kokotos and Dennis groups (**4**) as shown in Figure 1.[27−30] Of these inhibitors, there exist two docked structures in the GIVA PLA_2 active site, generated through computer modeling,[15,31] but there are no in depth examinations of the binding pocket contacts between inhibitor and enzyme.

The pyrrolidine-derived inhibitor pyrrophenone displays some of the best inhibition but (due to chemical properties) is not useful as a drug.[18] We have previously shown that the 2-oxoamide compounds show an antihyperalgesic effect in rat models.[32] The invention of better 2-oxoamide inhibitors is a promising drug strategy, and, to such end, we set out to model the 2-oxoamide inhibitor AX007, as well as the pyrrolidine-derived inhibitor pyrrophenone, bound in the active site. This required a technique to monitor changes in protein structure upon inhibitor binding.

Peptide amide hydrogen−deuterium exchange analyzed via liquid chromatography/mass spectrometry has been widely used

(12) Liu, S.; Laliberte, F.; Falgueyret, J. P.; Street, I.; Huang, Z. *FASEB J.* **1995**, *9*, A1310−A1310.
(13) Riendeau, D.; Guay, J.; Weech, P. K.; Laliberte, F.; Yergey, J.; Li, C.; Desmarais, S.; Perrier, H.; Liu, S.; Nicoll-Griffith, D. *J. Biol. Chem.* **1994**, *269*, 15619–15624.
(14) Trimble, L. A.; Street, I. P.; Perrier, H.; Tremblay, N. M.; Weech, P. K.; Bernstein, M. A. *Biochemistry* **1993**, *32*, 12560–12565.
(15) McKew, J. C.; Lovering, F.; Clark, J. D.; Bemis, J.; Xiang, Y.; Shen, M.; Zhang, W.; Alvarez, J. C.; Joseph-McCarthy, D. *Bioorg. Med. Chem. Lett.* **2003**, *13*, 4501–4.
(16) McKew, J. C.; Foley, M. A.; Thakker, P.; Behnke, M. L.; Lovering, F. E.; Sum, F. W.; Tam, S.; Wu, K.; Shen, M. W.; Zhang, W.; Gonzalez, M.; Liu, S.; Mahadevan, A.; Sard, H.; Khor, S. P.; Clark, J. D. *J. Med. Chem.* **2006**, *49*, 135–58.
(17) Lee, K. L.; Foley, M. A.; Chen, L.; Behnke, M. L.; Lovering, F. E.; Kirincich, S. J.; Wang, W.; Shim, J.; Tam, S.; Shen, M. W.; Khor, S.; Xu, X.; Goodwin, D. G.; Ramarao, M. K.; Nickerson-Nutter, C.; Donahue, F.; Ku, M. S.; Clark, J. D.; McKew, J. C. *J. Med. Chem.* **2007**, *50*, 1380–400.
(18) McKew, J. C.; Lee, K. L.; Shen, M. W.; Thakker, P.; Foley, M. A.; Behnke, M. L.; Hu, B.; Sum, F. W.; Tam, S.; Hu, Y.; Chen, L.; Kirincich, S. J.; Michalak, R.; Thomason, J.; Ipek, M.; Wu, K.; Wooder, L.; Ramarao, M. K.; Murphy, E. A.; Goodwin, D. G.; Albert, L.; Xu, X.; Donahue, F.; Ku, M. S.; Keith, J.; Nickerson-Nutter, C. L.; Abraham, W. M.; Williams, C.; Hegen, M.; Clark, J. D. *J. Med. Chem.* **2008**, *51*, 3388–413.
(19) Seno, K.; Okuno, T.; Nishi, K.; Murakami, Y.; Watanabe, F.; Matsuura, T.; Wada, M.; Fujii, Y.; Yamada, M.; Ogawa, T.; Okada, T.; Hashizume, H.; Kii, M.; Hara, S.; Hagishita, S.; Nakamoto, S.; Yamada, K.; Chikazawa, Y.; Ueno, M.; Teshirogi, I.; Ono, T.; Ohtani, M. *J. Med. Chem.* **2000**, *43*, 1041–1044.
(20) Seno, K.; Okuno, T.; Nishi, K.; Murakami, Y.; Yamada, K.; Nakamoto, S.; Ono, T. *Bioorg. Med. Chem. Lett.* **2001**, *11*, 587–590.
(21) Ono, T.; Yamada, K.; Chikazawa, Y.; Ueno, M.; Nakamoto, S.; Okuno, T.; Seno, K. *Biochem. J.* **2002**, *363*, 727–735.
(22) Flamand, N.; Picard, S.; Lemieux, L.; Pouliot, M.; Bourgoin, S. G.; Borgeat, P. *Br. J. Pharmacol.* **2006**, *149*, 385–392.
(23) Connolly, S.; Bennion, C.; Botterell, S.; Croshaw, P. J.; Hallam, C.; Hardy, K.; Hartopp, P.; Jackson, C. G.; King, S. J.; Lawrence, L.; Mete, A.; Murray, D.; Robinson, D. H.; Smith, G. M.; Stein, L.; Walters, I.; Wells, E.; Withnall, W. J. *J. Med. Chem.* **2002**, *45*, 1348–1362.
(24) Ludwig, J.; Bovens, S.; Brauch, C.; Elfringhoff, A. S.; Lehr, M. *J. Med. Chem.* **2006**, *49*, 2611–2620.
(25) Hess, M.; Elfringhoff, A. S.; Lehr, M. *Bioorg. Med. Chem.* **2007**, *15*, 2883–2891.
(26) Fritsche, A.; Elfringhoff, A. S.; Fabian, J.; Lehr, M. *Bioorg. Med. Chem.* **2008**, *16*, 3489–3500.
(27) Kokotos, G.; Kotsovolou, S.; Six, D. A.; Constantinou-Kokotou, V.; Beltzner, C. C.; Dennis, E. A. *J. Med. Chem.* **2002**, *45*, 2891–2893.
(28) Kokotos, G.; Six, D. A.; Loukas, V.; Smith, T.; Constantinou-Kokotou, V.; Hadjipavlou-Litina, D.; Kotsovolou, S.; Chiou, A.; Beltzner, C. C.; Dennis, E. A. *J. Med. Chem.* **2004**, *47*, 3615–3628.
(29) Stephens, D.; Barbayianni, E.; Constantinou-Kokotou, V.; Peristeraki, A.; Six, D. A.; Cooper, J.; Harkewicz, R.; Deems, R. A.; Dennis, E. A.; Kokotos, G. *J. Med. Chem.* **2006**, *49*, 2821–2828.
(30) Six, D. A.; Barbayianni, E.; Loukas, V.; Constantinou-Kokotou, V.; Hadjipavlou-Litina, D.; Stephens, D.; Wong, A. C.; Magrioti, V.; Moutevelis-Minakakis, P.; Baker, S. F.; Dennis, E. A.; Kokotos, G. *J. Med. Chem.* **2007**, *50*, 4222–4235.
(31) Gopalsamy, A.; Yang, H.; Ellingboe, J. W.; McKew, J. C.; Tam, S.; Joseph-McCarthy, D.; Zhang, W.; Shen, M.; Clark, J. D. *Bioorg. Med. Chem. Lett.* **2006**, *16*, 2978–81.
(32) Yaksh, T. L.; Kokotos, G.; Svensson, C. I.; Stephens, D.; Kokotos, C. G.; Fitzsimmons, B.; Hadjipavlou-Litina, D.; Hua, X. Y.; Dennis, E. A. *J. Pharmacol. Exp. Ther.* **2006**, *316*, 466–475.

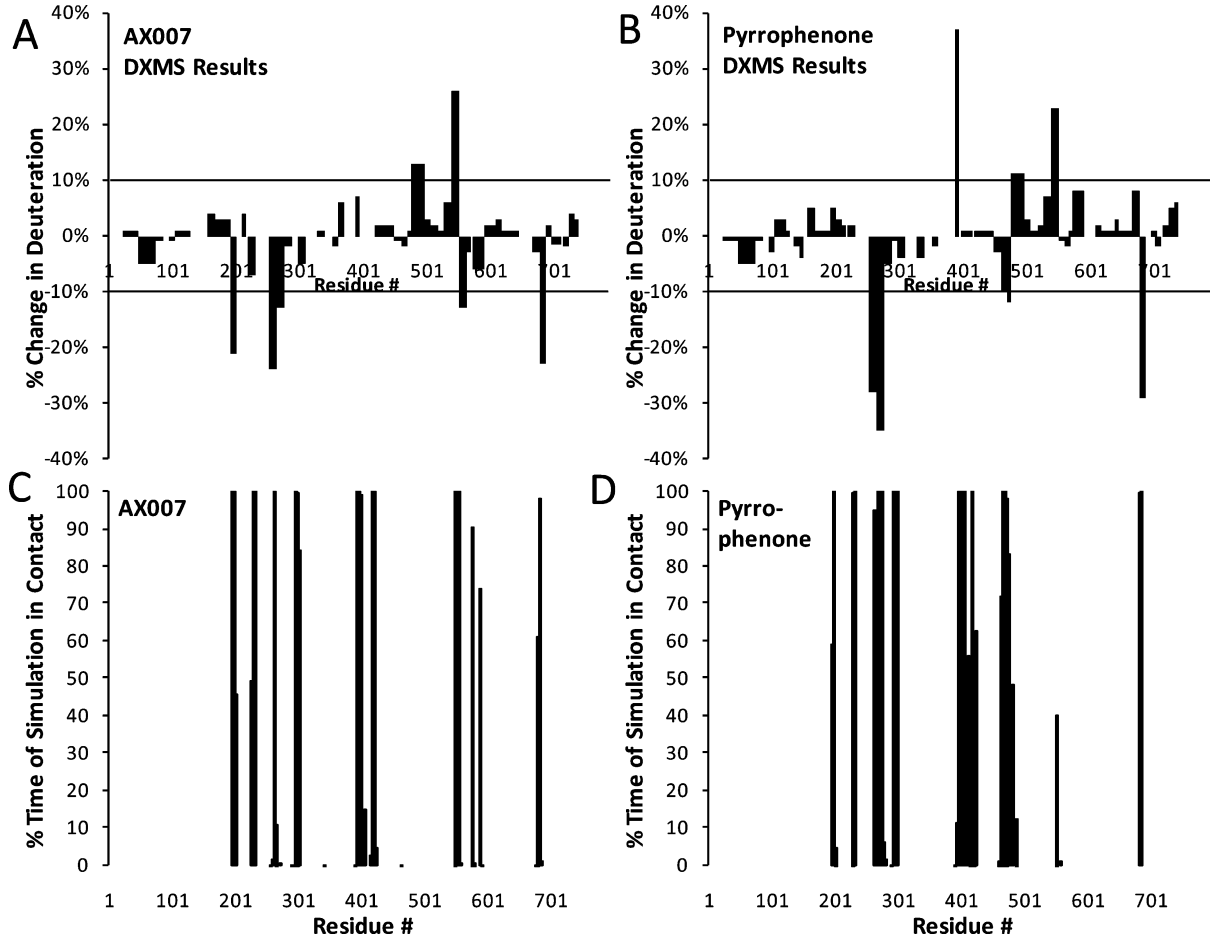

Figure 2. Deuterium exchange information as compared to computer simulation results. Panels A and B: The percent change in deuterium exchange between inhibitor free GIVA PLA_2 and oxoamide-bound (panel A) or pyrrophenone-bound (panel B) GIVA PLA_2 at 100 s of on-exchange is shown. Each bar represents a region in which deuterium exchange was quantified. All changes greater than 10% are considered significant. Panels C and D: The percent chance of specific residues that were within 5 Å of the docked inhibitor in the molecular dynamics simulation is plotted for oxoamide-bound (panel C) and pyrrophenone-bound (panel D) PLA_2.

to analyze protein−protein interactions,[33,34] protein conformational changes,[35,36] and protein dynamics.[37] We have previously used this technique to explore changes in lipid binding with the GIVA PLA_2 and discovered changes in exchange profiles in the presence of the irreversible inhibitor MAFP.[11] The DXMS technique, in conjunction with site-directed mutagenesis, has recently been used to identify regions interacting with different inhibitors.[38,39]

Coupled with these experimental techniques, computational methods can be employed to study the atomic-level details in the GIVA PLA_2−inhibitor complex. Extensive simulations of the phospholipase A_2's have been carried out. Most notably, Wee et al. recently conducted a coarse-grained simulation of the pancreatic phospholipase A_2, in which they demonstrate how the enzyme adheres to the lipid bilayer.[40] Quantum mechanical methodologies have also been applied to the phospholipase system.[41] This work has proven vital to the understanding of phospholipase A_2 chemistry and dynamics.

In turn, by running molecular dynamics (MD) simulations of GIVA PLA_2 with inhibitor, one can observe how the latter docks into and stabilizes itself in the enzyme. Contacts between the inhibitor and specific residues of GIVA PLA_2 can also be identified. This information augments the results from the deuterium exchange technique, which at this time lacks the resolution to achieve single-residue data. In lieu of known crystal structures depicting the enzyme−inhibitor complex, this computational work affords working models of the complexes and characterizes key enzyme−inhibitor interactions. The MD simulations and subsequent analysis aid in drawing comparisons between the oxoamide and pyrrophenone complexes.

The study of these two very different inhibitors provides an excellent model for generalized GIVA PLA_2 inhibition. The dual techniques of deuterium exchange mass spectrometry and MD simulation are excellent methods to probe the dynamical changes induced by binding of inhibitors to any enzyme. This study also

(33) Hamuro, Y.; Anand, G. S.; Kim, J. S.; Juliano, C.; Stranz, D. D.; Taylor, S. S.; Woods, V. L., Jr. *J. Mol. Biol.* **2004**, *340*, 1185–96.
(34) Mandell, J. G.; Falick, A. M.; Komives, E. A. *Proc. Natl. Acad. Sci. U.S.A.* **1998**, *95*, 14705–10.
(35) Brudler, R.; Gessner, C. R.; Li, S.; Tyndall, S.; Getzoff, E. D.; Woods, V. L., Jr. *J. Mol. Biol.* **2006**, *363*, 148–160.
(36) Hoofnagle, A. N.; Resing, K. A.; Goldsmith, E. J.; Ahn, N. G. *Proc. Natl. Acad. Sci. U.S.A.* **2001**, *98*, 956–61.
(37) Wales, T. E.; Engen, J. R. *Mass Spectrom. Rev.* **2006**, *25*, 158–170.
(38) Brier, S.; Lemaire, D.; DeBonis, S.; Forest, E.; Kozielski, F. *J. Mol. Biol.* **2006**, *360*, 360–376.
(39) Brier, S.; Lemaire, D.; DeBonis, S.; Kozielski, F.; Forest, E. *Rapid Commun. Mass Spectrom.* **2006**, *20*, 456–462.
(40) Wee, C. L.; Balali-Mood, K.; Gavaghan, D.; Sansom, M. S. P. *Biophys. J.* **2008**, *95*, 1649–1657.
(41) Bala, P.; Grochowski, P.; Nowinski, K.; Lesyng, B.; McCammon, J. A. *Biophys. J.* **2000**, *79*, 1253–1262.

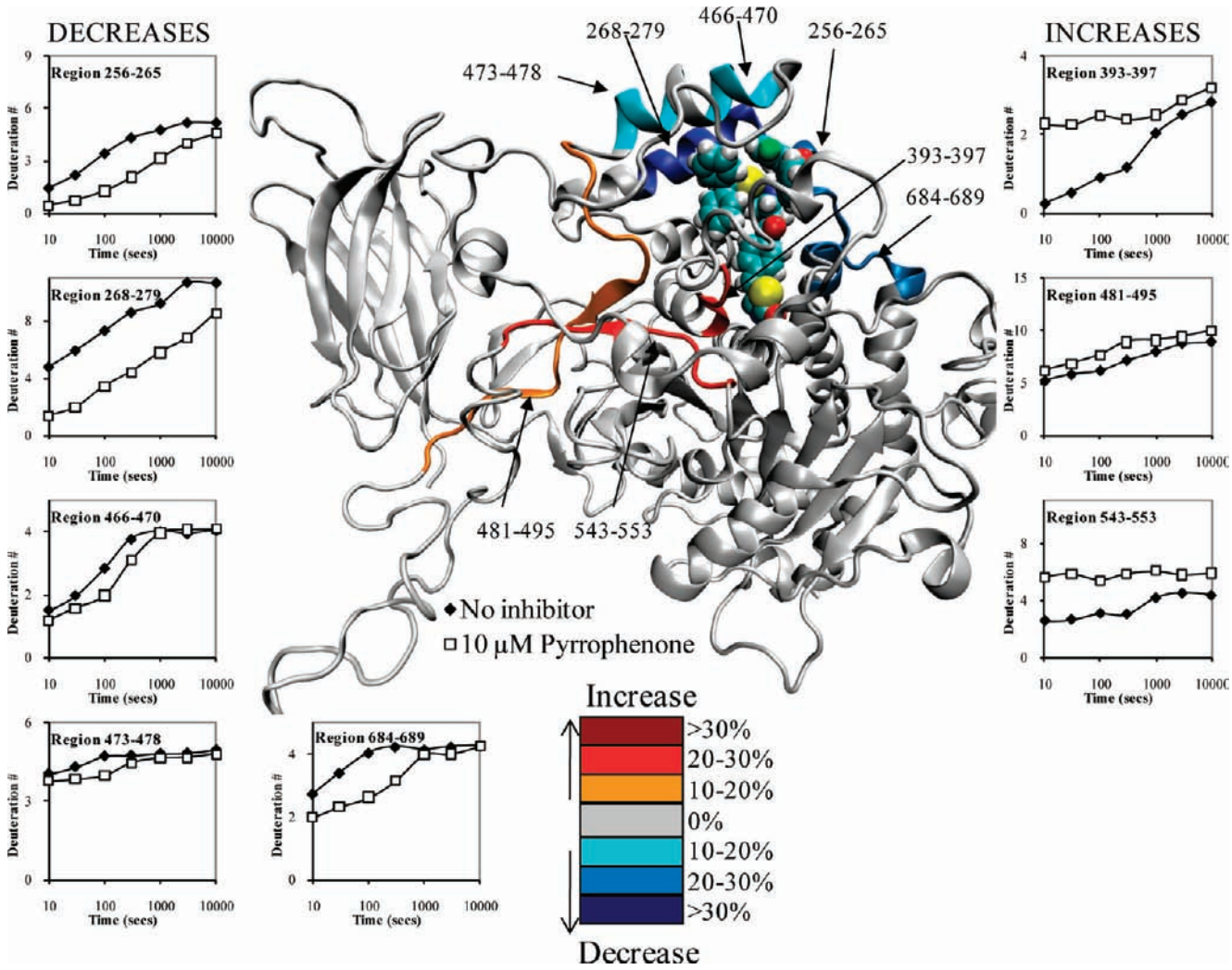

Figure 3. Deuterium exchange upon binding of 10 μM pyrrophenone. The number of incorporated deuterons at seven time points in eight different regions, 256−265, 268−279, 393−397, 466−470, 473−478, 481−495, 543−553, and 684−689, in GIVA PLA2 are plotted onto the docked model of pyrrophenone binding at 50 ns of simulation time (the inhibitor is shown in space-filled form). Decreases or increases in deuteration greater than 10% at the 100 s time point are represented by the color scheme in the legend.

represents a continuation of our deuterium exchange studies on the PLA_2 family of enzymes.[11,42,43] We have identified specific regions of the protein that interact with the oxoamide and pyrrophenone inhibitors, and we have carried out extensive computer simulations to create a model of inhibitor binding in the active site. We have also identified significant differences in the way pyrrophenone and oxoamide bind GIVA PLA_2. This work leads to the possibilities of enhanced rational drug design through the powerful combination of experimental and computational work.

Materials and Methods

All reagents were analytical reagent grade or better. Pyrrophenone was the generous gift from Shionogi, and the 2-oxoamide AX007 was synthesized as described.[28]

Protein Expression and Purification. The C-terminal His6-tagged GIVA PLA2 was expressed using recombinant baculovirus in a suspension culture of Sf9 insect cells. The cell pellet was lysed in 25 mM Tris-HCl pH 8.0, 150 mM NaCl, 2 mM β-mercaptoethanol, and 2 mM EGTA, and then the insoluble portion was removed by centrifugation at 12 000*g* for 30 min. The supernatant was passed through a column comprised of 6 mL of nickel−nitrilotriacetic acid agarose (Qiagen, Valencia, CA). The protein in the native state was eluted in the "protein buffer" (25 mM Tris-HCl pH 8.0, 100 mM NaCl, 125 mM imidazole, and 2 mM dithiothreitol). The protein concentration was measured using the Bradford assay (Biorad) to manufacturer's standards, and the activity was assayed using mixed micelles in a modified Dole assay.[44] Purified GIVA PLA_2 (2 mg/mL) was stored in the protein buffer on ice for DXMS experiments. Experiments were performed immediately after elution from the nickel column.

Preparation of Deuterated Samples for On-Exchange Experiments. D_2O buffer contained 10 mM Tris (pD 7.5), 50 mM NaCl in 98% D_2O. Hydrogen/deuterium exchange experiments were initiated by mixing 20 μL of GIVA PLA_2 (containing 40 μg) in protein buffer with 60 μL of D_2O buffer to a final concentration of 73% D_2O at pH 7.5. In inhibitor binding experiments, the GIVA PLA_2 in protein buffer was preincubated in the presence of 40 μM pyrrophenone, 40 μM oxoamide AX007, or DMSO control. The

(42) Burke, J. E.; Karbarz, M. J.; Deems, R. A.; Li, S.; Woods, V. L., Jr.; Dennis, E. A. *Biochemistry* **2008**, *47*, 6451–9.
(43) Hsu, Y. H.; Burke, J. E.; Stephens, D. L.; Deems, R. A.; Li, S.; Asmus, K. M.; Woods, V. L., Jr.; Dennis, E. A. *J. Biol. Chem.* **2008**, *283*, 9820–7.
(44) Lucas, K. K.; Dennis, E. A. *Prostaglandins Other Lipid Mediators* **2005**, *77*, 235–48.

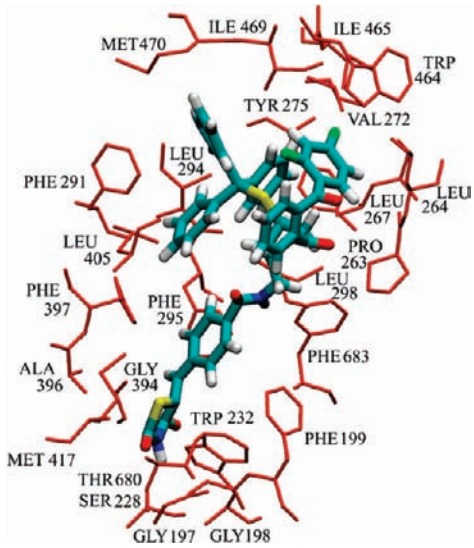

Figure 4. Residues involved in binding pyrrophenone. The residues that have contact with pyrrophenone greater than 90% of the time in the molecular dynamics simulation are represented as red sticks and labeled in the figure. The inhibitor is shown in the licorice representation, with carbon, hydrogen, oxygen, nitrogen, and phosphorus atoms colored cyan, white, red, blue, and yellow, respectively.

inhibitors were added from 600 μM stock dissolved in DMSO. The final concentration of DMSO was 1.5% for all experiments. The inhibitors were allowed to preincubate with the enzyme for 10 min at 23 °C before addition of D_2O buffer. The D_2O buffer was added, and the samples were incubated at 23 °C for an additional 10, 30, 100, 300, 1000, 3000, or 10 000 s. The dilution of inhibitors with D_2O buffer gave a final inhibitor concentration of 10 μM. The deuterium exchange was quenched by adding 120 μL of ice-cold quench solution (0.96% formic acid, 1.66 M guanidine hydrochloride (GdHCl)) that acidified the sample to a final pH = 2.5 and concentrations of formic acid of 0.58% and 1 M GdHCl. The samples were placed on ice for 10 min to partially denature the protein and obtain optimal peptide maps. Vials with frozen samples were stored at −80 °C until analysis, usually within 3 days.

Proteolysis−Liquid-Chromatography−Mass Spectrometry Analysis of Samples. All steps were performed at 0 °C as previously described.[11,33,35]

Data Processing. SEQUEST software (Thermo Finnigan Inc.) was used to identify the sequence of the peptide ions as previously described.[11] DXMS Explorer (Sierra Analytics Inc., Modesto, CA) was used for the analysis of the mass spectra, and all data processing was the same as previously described.[11,33,35] The deuteration level of each peptide was calculated by the ratio of the incorporated deuteron number to the maximum possible deuteration number. Peptide deuteration levels in replicate samples, measured by our DXMS methods, have been found to vary by less than 10%, and we therefore regard changes greater than 10% as significant.[33] All experiments were performed at least twice, and representative data are shown. Trends in the data were similar from experiment to experiment, but total deuterium content varied by roughly 5−10% in similar experiments carried out weeks apart. For all peptides shown in the figures, different peptides that cover the same region are included in the Supporting Information as Figure 1.

Molecular Dynamics Simulations. In total, three systems were simulated: the apo form of GIVA PLA_2, GIVA PLA_2 with pyrrophenone bound, and GIVA PLA_2 with oxoamide bound. The structure of GIVA PLA_2 was obtained from the Protein Data Bank (code 1CJY).[10] In this reported structure, several segments were missing including residues 407−414, 431−462, 498−538, and 626−632. These apparently flexible regions were modeled into chain B of 1CJY using SWISS MODEL (Supporting Information Figure 2).[45] The resulting complete structure of GIVA PLA_2 was optimized by 500 steps each of steepest decent and conjugate gradient energy minimizations and used in all three systems.

The inhibitors pyrrophenone and oxoamide were constructed using the Accelrys Discovery Studio package, in which they were built and energy minimized to obtain their initial conformations. Each inhibitor was manually placed in the active site of GIVA PLA_2 using the aforementioned knowledge of the active site and residues implicated in binding. This was carried out using the Visual Molecular Dynamics (VMD) package,[46] which was also used for further construction of all three systems. The protein (or the protein−inhibitor complex) was placed in a simulation box of dimensions 127 × 73 × 91 Å, solvated with approximately 22 750 TIP3P water molecules, and neutralized with 28 sodium counterions (~80 000 atoms total for each system).

The minimization steps and all subsequent simulations were carried out using the NAMD molecular dynamics package.[47] For the apo structure, an energy minimization was performed on the system first with the protein backbone atoms fixed, for 25 000 steps, to allow the water/ions to conform to the shape of the protein, and then with no such constraint, for another 25 000 steps, to relieve any unfavorable contacts in the entire system. For the inhibitor-bound systems, a similar energy minimization scheme was performed, with the addition of an extra minimization holding the inhibitor coordinates fixed, to relieve unfavorable contacts between the inhibitor and protein. For all three systems, a heating step was performed, in which the system was gradually heated (~50 ps) to a temperature of 300 K. During this heating and then the equilibration phase, the protein backbone and inhibitor atoms were restrained with a force constant of 5 kcal mol^{-1} $Å^{-2}$. In the equilibration phase, pressure coupling was added, and a series of restrained MD simulations were conducted. The restraints were gradually relieved, and the free, unrestrained system was equilibrated for 1 ns further. The production runs for each system commenced; each protein (or protein−inhibitor complex) was simulated for 50 ns.

For each of the production runs, the temperature was maintained at 300 K using the Langevin thermostat, with a coupling constant of 2 ps^{-1}. Pressure was maintained at 1.01325 kPa using the Langevin piston method, with the "GroupPressure" and "FlexibleCell" parameters turned on. Bonds to hydrogen atoms were held fixed while using a 2 fs time step. Nonbonded interactions and full electrostatics were calculated every 1 and 2 steps, respectively. Nonbonded interactions were smoothly switched off between 8.5 and 10 Å, while the cutoff for pairlist distance was set to 12 Å. Long-range electrostatic forces were evaluated using the particle mesh Ewald (PME) method.[48] The CHARMM22/27 all-hydrogen parameter files were used for protein and inhibitors in all three simulations.[49] The standard protein/amino acid parameters were used for GIVA PLA_2 and pyrrophenone (by analogy to various

(45) Peitsch, M. C. *Biochem. Soc. Trans.* **1996**, *24*, 274–279.
(46) Humphrey, W.; Dalke, A.; Schulten, K. *J. Mol. Graphics* **1996**, *14*, 33–38.
(47) Phillips, J. C.; Braun, R.; Wang, W.; Gumbart, J.; Tajkhorshid, E.; Villa, E.; Chipot, C.; Skeel, R. D.; Kalé, L.; Schulten, K. *J. Comput. Chem.* **2005**, *26*, 1781–1802.
(48) Essmann, U.; Perera, L.; Berkowitz, M. L.; Darden, T.; Lee, H.; Pedersen, L. G. *J. Chem. Phys.* **1995**, *103*, 8577–8593.
(49) MacKerell, A. D.; Bashford, D.; Bellott, M.; Dunbrack, R. L.; Evanseck, J. D.; Field, M. J.; Fischer, S.; Gao, J.; Guo, H.; Ha, S.; Joseph-McCarthy, D.; Kuchnir, L.; Kuczera, K.; Lau, F. T. K.; Mattos, C.; Michnick, S.; Ngo, T.; Nguyen, D. T.; Prodhom, B.; Reiher, W. E.; Roux, B.; Schlenkrich, M.; Smith, J. C.; Stote, R.; Straub, J.; Watanabe, M.; Wiorkiewicz-Kuczera, J.; Yin, D.; Karplus, M. *J. Phys. Chem. B* **1998**, *102*, 3586–3616.

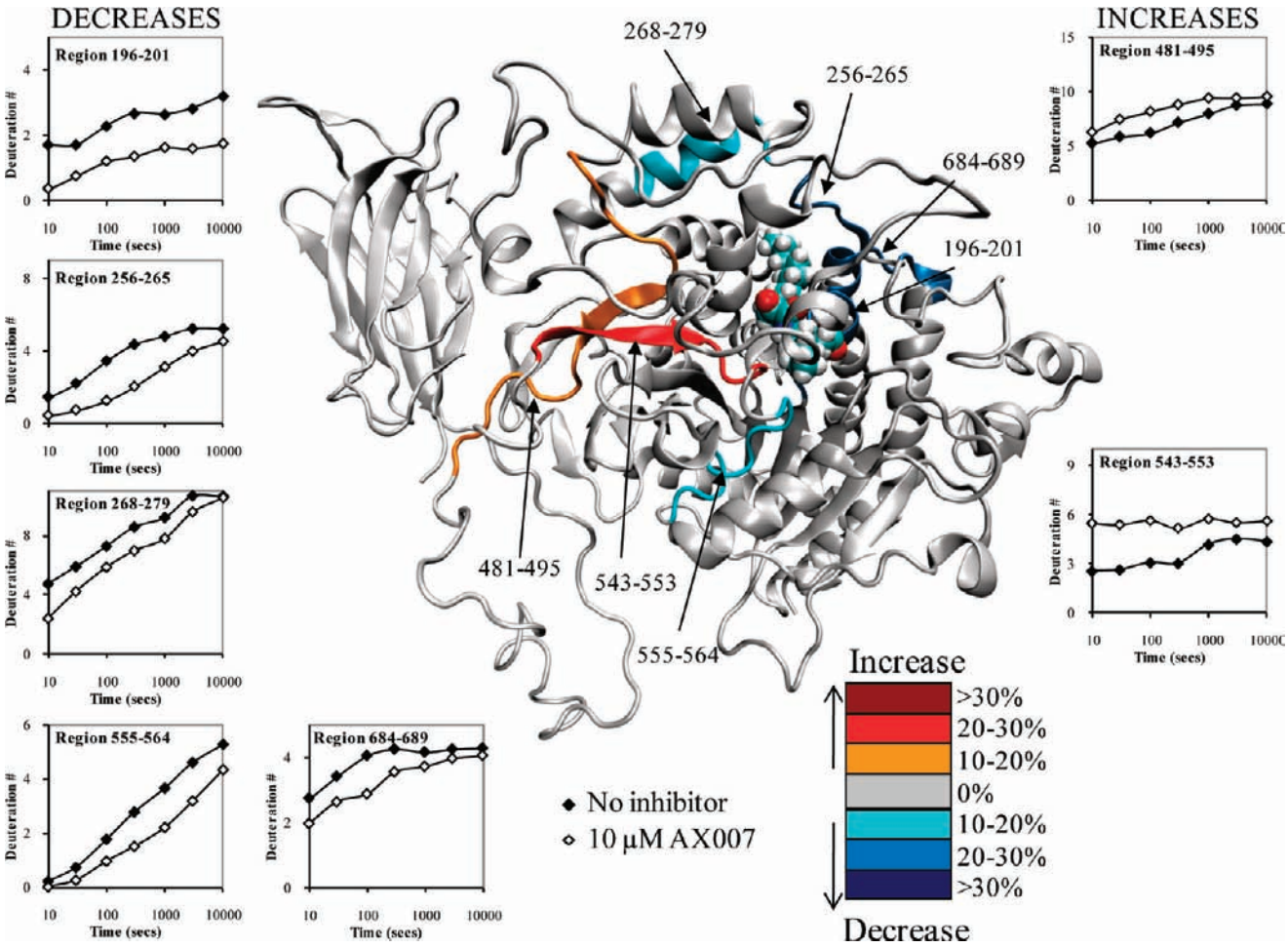

Figure 5. Deuterium exchange upon binding of 10 μM AX007. The number of incorporated deuterons at seven time points in seven different regions, 196−201, 256−265, 268−279, 555−564, 481−495, 543−553, and 684−689, in GIVA PLA2 are plotted onto the docked model of the oxoamide AX007 binding at 50 ns of simulation time (the inhibitor is shown in space-filled form). Decreases or increases in deuteration greater than 10% at the 100 s time point are represented by the color scheme in the legend.

amino acid side chain structures). The oxoamide was parametrized according to the lipid parameters provided in CHARMM27.

Results and Discussion

GIVA PLA2 Digestion Map. The protein digestion procedure was optimized to produce a peptide map that yielded the best coverage of GIVA PLA_2 as described previously.[11,43] The optimized condition identified 185 distinct peptides that gave 94% coverage of the GIVA PLA_2 sequence (Supporting Information Figure 3). From this group, the 71 peptides with the best signal-to-noise ratio with the least amount of redundant data were used to generate the figures as described previously.[11,43] All peptides were analyzed for deuterium content as a comparison, but only the ones with nonredundant data were used in the generation of figures. Additional peptides that overlap regions shown in the figures are shown in Supporting Information Figure 1.

Modeling and Simulation. The overall structure of the protein remained close to the crystal structure in all three simulations (Supporting Information Figure 4). The regions missing in the X-ray structure, but model-built in the simulations, exhibited large fluctuations throughout the simulations, which is consistent with their being disordered in the crystals. However, the majority of the modeled regions remained solvated, without making significant contact with the rest of the protein. As a result, their motion did not affect the active site region of the enzyme. In the apo form, GIVA PLA_2 shows no significant conformational changes, as expected. In the inhibitor-bound forms, both pyrrophenone and the oxoamide show considerable movement in the first half of simulation but settle to a converged conformation and location in the last 25 ns, as judged by the root-mean-square (rmsd) of the inhibitors (see Supporting Information Figure 4). Thus, the last 25 ns of each simulation was used in all subsequent simulation analyses.

GIVA PLA_2 Pyrrophenone Binding Experiments. We examined both the pyrrolidine-derived inhibitor pyrrophenone as well as the 2-oxoamide-derived inhibitor AX007. These compounds are structurally quite different and target different functionalities of the GIVA PLA_2. Therefore, determining exactly how these inhibitors bind is an important goal, because it allows the possibility of combining the best parts of each inhibitor to form new, more effective inhibitors to allow for further structure−activity studies. On-exchange experiments were performed on the intact GIVA PLA_2 enzyme in the presence of both 10 μM pyrrophenone and 10 μM of the 2-oxoamide inhibitor AX007 to determine if inhibitor binding caused changes in deuterium exchange rates. Theexperiments were carried out at relatively low ratios of protein to inhibitor (1:2) in 1.5% DMSO to prevent possible complications from inhibitor aggregation and misleading deuterium exchange results. Because interfacial enzymes

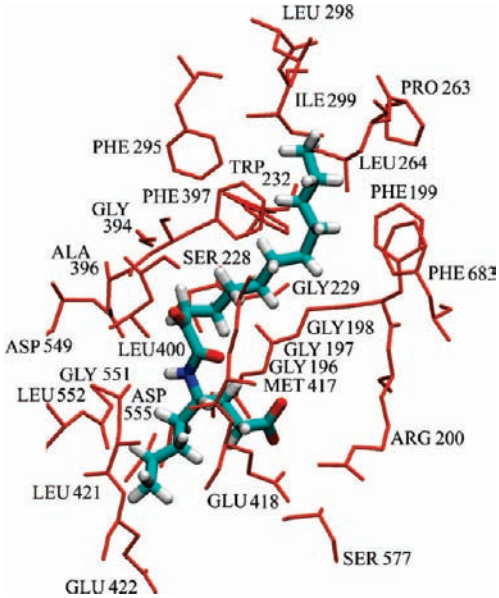

Figure 6. Residues involved in the binding of oxoamide AX007. The residues that have contact with the oxoamide greater than 90% of the time in the molecular dynamics simulation are represented as red sticks and labeled on the figure. The inhibitor is shown in the licorice representation, with carbon, hydrogen, oxygen, nitrogen, and phosphorus atoms colored cyan, white, red, blue, and yellow, respectively.

act on a two dimensional surface, the K_d value of the inhibitors was difficult to determine. In previous kinetic studies, the IC50 levels for pyrrophenone and AX007 were determined to be 0.11 and 3.5 μM, respectively. We used 10 μM for both inhibitors to insure adequate binding of the inhibitors to protein, but we were limited from adding more due to the tendencies of both inhibitors to form large hydrophobic aggregates in solution. Experiments were carried out at seven time points varyingfrom 10 to 10 000 s. Both inhibitors showed multiple regions of the protein with greater than 10% change in the on-exchange rates between the inhibitor-bound and apo forms at all time points. These percent increases and decreases in on-exchange rates showed a strong correlation with computationaldata mapping percent chance of contact per residue number (Figure 2). The residues from 292−298 and 401−417 predicted to be in contact with the inhibitor (within 5 Å) from modeling and that show no changes in deuterium exchange are all located in regions with either extremely slow or rapid exchange, and hence there is no significant difference in exchange between apo- and haloforms (see Supporting Information Figure 5). The difference in on-exchange at the 100 s time point captured all of the major changes and was used to generate thedata shown in Figures 2, 3, and 5.

The inhibitor pyrrophenone was synthesized in 2001[20] and contains a thiazoloidinedione ring postulated to target Arg-200 and a carbonyl group bridging the two benzoyl groups that is expected to target the active site Ser-228. This class of inhibitors was also shown, through structure−activity work, to have large increases in inhibitory potency with the addition of large bulky lipophilic substituents, suggesting the presence of a hydrophobic binding pocket in the enzyme.[19] Using deuterium exchange and modeling, we planned to test this hypothesis on the basis of structure−activity work.

Eight regions of the GIVA PLA_2 exhibited significant changes in deuterium exchange in the presence of pyrrophenone. Figure 3 shows these results both quantitatively and visually imposed on snapshots from the MD simulations. Three regions of the protein, residues 393−397, 481−495, and 543−553, exhibited increased rates of exchange in the presence of pyrrophenone. Regions 393−397 and 543−553 had greater differences in on-exchange rates (between apo- and pyrrophenone-bound enzymes) at early time points of roughly 20−30%, with the difference going to zero at later time points. Region 393−397 contains Ala-396 and Phe-397 in contact with pyrrophenone. Region 481−495 had a constant 10−15% increase in exchange at all time points. These are the exact regions that we have previously shown had increases in on-exchange rates in the presence of the potent irreversible GIVA PLA_2 inhibitor MAFP, as well as natural phospholipid substrate vesicles.[11] We have hypothesized that these regions show an increase in exchange due to the opening of the lid region from 415−432 and that pyrrophenone also causes an opening of the lid region upon binding in the active site. In turn, this opening event induces an increase in the solvent accessibility and results in higher on-exchange rates. This lid opening was not seen in our simulations, and this is most likely a time-dependent process that is too slow to view with molecular dynamics.

Five regions of the protein, residues 256−265, 268−279, 466−470, 473−478, and 684−689, demonstrated decreases in exchange between apo- and pyrrophenone-bound enzymes (Figure 3). Region 268−279 exhibits greater than 30% decreases in exchange at all time points. Correlating with the MD simulation, this region harbors multiple residues that are in constant contact with the pyrrophenone. Regions 256−265 and 684−689 exhibit 20−30% decreases at early time points and drop to less than 10% at later time points. These regions also contain multiple hydrophobic residues demonstrated by simulation to be in contact with pyrrophenone; yet, this is to a lesser extent (and thus less of a decrease in exchange) as compared to region 268−279. Regions 466−470 and 473−478 showed 10−15% decreases in on-exchange rates from 30 to 300 s but no differences in exchange at earlier or later time points. We assume that the deuterium exchange rates are a combination of the individual rates of numerous amide hydrogens. In region 466−470, the rate profile suggests there is a set of amide hydrogens that are not exchanged in either the apo or the inhibitor-bound structure at 30 s, and hence no difference in exchange is seen. At 100 and 300 s, these amide hydrogens are more deuterated in the apo structure and have lower levels of exchange in the inhibitor-bound structure due to decreases in solvent accessibility, which gives a 10−15% decrease. At 1000 s, however, these amides are fully exchanged in both the apo form and the inhibitor-bound form, which gives similar deuteration levels at this time point.

Our deuterium exchange results show decreases in exchange in numerous regions containing hydrophobic regions, and this matches our modeling work as shown in Figure 4, where Pro-263, Leu-264, Leu-267, Val-272, Tyr-275, Trp-464, Ile-465, Ile-469, Met-470, and Phe-683 all make contact with the numerous phenyl groups in pyrrophenone. In addition, region 282−291, which includes Phe-291, shows a constant 7% decrease across all time points and has been included in Supporting Information Figure 1. These residues most likely are acting as the hydrophobic pocket postulated through structure activity work with pyrrophenone, and our results correlate with recent data from Wyeth showing that GIVA PLA_2 inhibitors become more potent when the steric bulk of the inhibitor is increased in functionally allowed regions.[18] However, we find that the thiazoloidinedione functionality targets Ser-228, rather than targeting Arg-200, as

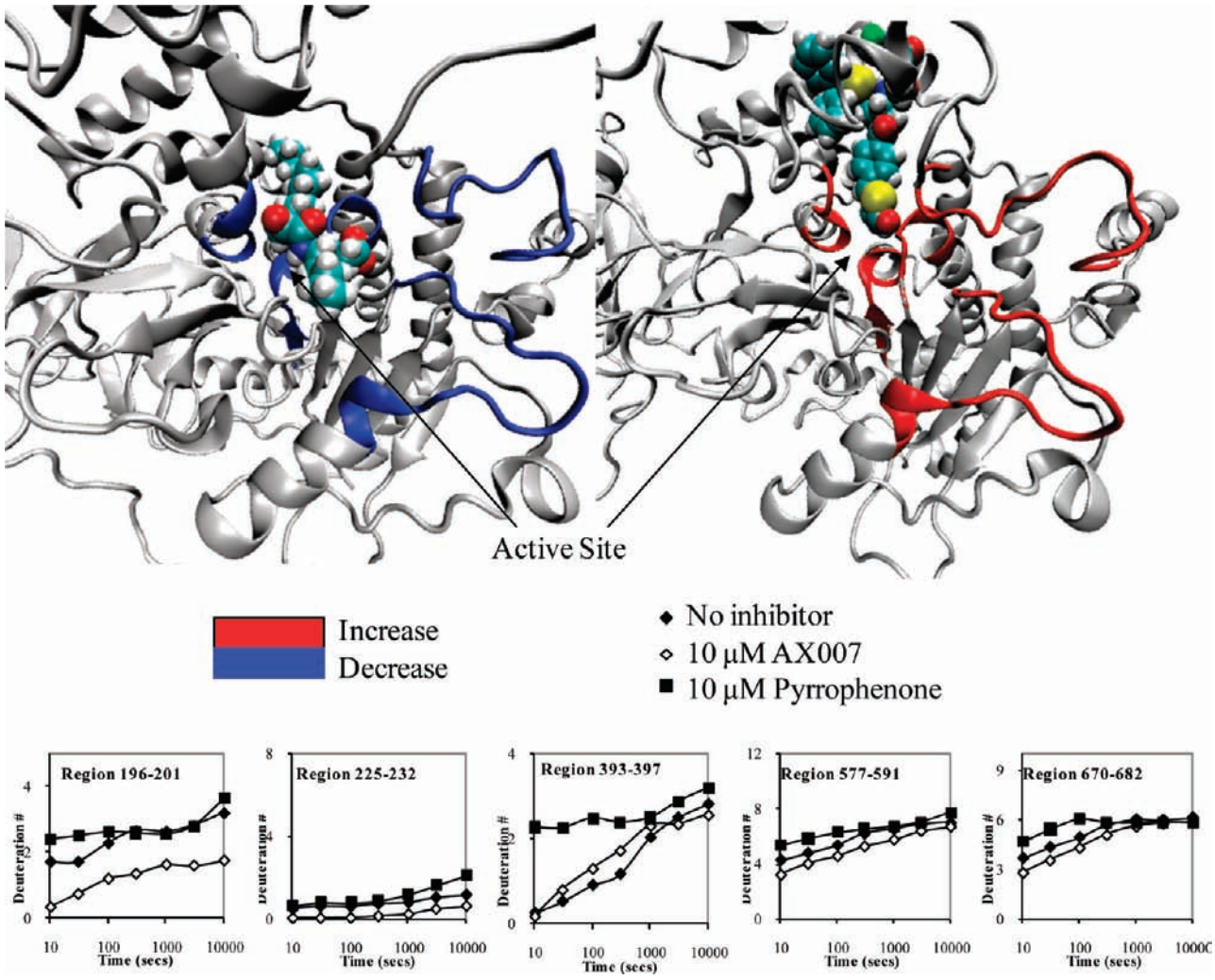

Figure 7. Different inhibitors cause different rates of exchange of the active site residues of GIVA PLA_2. The number of incorporated deuterons at seven time points in five different regions, 196−201, 225−232, 393−397, 577−591, and 670−682, in GIVA PLA2 are plotted onto the docked models. Areas that show both a greater than 10% change in exchange between oxoamide and pyrrophenone in at least three consecutive time points as well as less exchange with the oxoamide as compared to the apo structure (left), and more exchange with pyrrophenone as compared to the apo structure (right), are shown in color in the respective structures.

originally suggested by Shionogi,[19,20] with the carbonyl bridging the two phenyl groups in pyrrophenone being located at a large distance from the active site serine.

GIVA PLA_2 Oxoamide Binding Experiments. The 2-oxoamide inhibitor AX007 was originally synthesized and shown to be an effective GIVA PLA_2 inhibitor in 2002.[27] It was postulated to target GIVA PLA_2 via an interaction between its 2-oxo amide functionality and the active site Ser-228. Also, the carboxylic acid moiety of the oxoamide was designed to target Arg-200, while the inhibitor's long fatty acyl tail positions itself in the hydrophobic binding pocket.[28] Using deuterium exchange and modeling, we planned to test these hypothesis on the basis of structure−activity work.

Seven regions of the GIVA PLA_2 exhibited significant changes in deuterium exchange in the presence of the oxoamide (Figure 5). Two regions of the protein, residues 481−495 and 543−553, exhibit an increase in exchange in the presence of the oxoamide. These regions show the exact same deuterium on-exchange profile as the pyrrophenone-bound enzyme. However, the region 393−397 does not show any difference in exchange in the presence of the oxoamide. This result allows for multiple interpretations; perhaps the lid region is opened in a different way (as compared to the enzyme−pyrrophenone complex), thus only increasing solvent accessibility for regions 481−495 and 543−553, but not for region 393−397. Or, the lid region may be opened in the same way, but increased contacts between region 393−397 and the oxoamide cause a comparative decrease in exchange rates between the two inhibitor-bound structures.

Five regions of the protein, residues 196−201, 256−265, 268−279, 555−564, and 684−689, exhibit decreases in exchange in the presence of the oxoamide. Regions 256−265 and 684−689 reveal the same on-exchange pattern in the presence of both the oxoamide and the pyrrophenone. Simulation shows that along these regions, both inhibitors make similar hydrophobic contacts with Pro-263, Leu-264, and Phe-683 as shown in Figures 4 and 6. Region 268−279 has a 10−15% decrease in exchange at all time points, which is much lower than the corresponding differences in this region in the pyrrophenone−enzyme complex. This much smaller decrease in exchange in the oxoamide−enzyme complex correlates well with the simulation, which shows no residues in 268−279 making contacts with the inhibitor. Region 555−564 displays a 10−20% decrease in exchange at all time points in the presence of the oxoamide.

This region contains Asp-555 and neighbors Gly-551/Leu-552, all of which are in constant contact with the oxoamide during the simulation. Recent work by us has shown that the short, nonpolar, aliphatic R-group substituent on the oxoamide AX007 (residing on the linker between the 2-oxo and carboxylic acid) increased potency. We postulated that this is facilitated by a hydrophobic pocket in the enzyme that can accommodate this particular group.[28,30] The residues in and around 555−564 appear to constitute this pocket, as shown here by both on-exchange results and simulation. Region 196−201 exhibits a 20−30% decrease in exchange at all time points in the presence of the oxoamide. This region contains the proposed oxy-anion hole, residues Gly-196, Gly-197, Gly-198, Gly-229, and Arg-200, required for catalytic activity, as well as Phe-199, which is part of the hydrophobic pocket for the substrate. The modeling data show an interaction between the carboxylic acid of the oxoamide and Arg-200, as well as the carbonyl of the 2-oxoamide in contact with the oxyanion hole composed of the numerous glycine residues.

Differences in Oxoamide and Pyrrophenone Binding. Numerous regions of the protein show the same decreases or increases in exchange with both pyrrophenone and the oxoamide AX007. These regions include 256−265, 481−495, 543−553, and 684−689, and they all show similar contacts in these regions between both AX007 and pyrrophenone as shown in Figures 4 and 6. There are also regions such as 466−470, 473−478, and 555−564, which show changes only in the presence of one or the other inhibitor, and this is explained by specific contacts only seen between pyrrophenone or the oxoamide and the protein.

However, region 196−201 acts as an interesting example of the differences between pyrrophenone and oxoamide inhibitor binding. There are four different regions in the enzyme 196−201, 225−232, 577−591, and 670−682 that show a greater than 10% change in exchange between the pyrrophenone-bound structure and the oxoamide-bound structure (Figure 7). Many of these peptides do not show a change in deuterium exchange greater than 10% as compared to the apo structure. However, the comparison between pyrrophenone and the oxoamide does show a greater than 10% change in exchange. These peptide regions are all in or near the active site of the enzyme. Region 225−232, which contains the active site residue Ser-228, never exchanges greater than 25% at any time point. Yet, there is a greater than 10% change in exchange between the oxoamide and pyrrophenone-bound studies, with the oxoamide−enzyme complex showing less exchange than the pyrrophenone-bound sample.

For regions 577−591 and 670−682, the main effects are most likely localized to 577−580 and 680−682, respectively, which are located within 5 Å of the active site. These results show that the 2-oxoamide inhibitor AX007 decreases the solvent accessibility of the active site while pyrrophenone has the opposite effect (an increase). These results suggest an increase in flexibility of the active site in the presence of pyrrophenone with a concurrent decrease in flexibility in the presence of the oxoamide. This result also explains why there are numerous residues shown in contact with pyrrophenone in Figure 4 that do not have a decrease in exchange, due to increases in exchange caused by increased flexibility in the active site that counters decreases in exchange caused by inhibitor binding decreasing solvent accessibility. These results also help to explain why region 393−397 has an increase in exchange with pyrrophenone and not with the oxoamide. This region is located near the active site, and increases in exchange are seen with the presence of pyrrophenone, MAFP, and natural phospholipid substrate,[11] but not the oxoamide. The decreased solvent accessibility and lack of flexibility of the active site in the presence of the oxoamide would explain the lack of exchange increases in region 393−397. From viewing Figure 7, it is also apparent that the oxoamide mainly occupies the active site area, while pyrrophenone is mainly bound in the cap region near the interfacial binding surface of the enzyme.

Conclusions

These results have greatly enhanced our knowledge of how these two different inhibitors bind GIVA PLA_2 and have allowed us to model all of the residues contacting both inhibitors. This will allow us to create new inhibitors combining the 2-oxoamide functionality with a bulky lipophilic substituent in place of the acyl fatty acid tail to mimic how pyrrophenone binds GIVA PLA_2 through multiple hydrophobic contacts located on or near the cap region. This study is the first to combine deuterium exchange mass spectrometry with molecular dynamics simulations for the determination of inhibitor binding. This methodology provides an exciting new tool to develop better inhibitors, and we plan to continue this work through the synthesis and testing of new GIVA PLA_2 inhibitors based on our results.

Acknowledgment. We thank Dr. Howard Hsu for constructive review of this manuscript. We also thank the following agencies for funding: NIH GM20501 (E.A.D.), and CA099835, CA118595, GM037684, AI0220221, AI022160 (V.L.W.); a Discovery Grant (UC10591) from the University of California Industry-University Cooperative Research Program (V.L.W.); and NIH GM31749 and NSF Grants MCB-0506593 and MCA93S013 (J.A.M.). This work was also supported by the Howard Hughes Medical Institute, San Diego Supercomputing Center, the W.M. Keck Foundation, Accelrys, Inc., the National Biomedical Computational Resource, and the Center for Theoretical Biological Physics.

Supporting Information Available: Additional experimental information on peptide maps, computational modeling, and supporting data. This material is available free of charge via the Internet at http://pubs.acs.org.

JA900098Y